BIOCHEMISTRY
including biophysical chemistry & molecular biology
Article

Biochemistry **2010,** *49,* 5455–5463 5455
DOI: 10.1021/bi1006805

Characterization of an FMO Variant of *Chlorobaculum tepidum* Carrying Bacteriochlorophyll *a* Esterified by Geranylgeraniol†

Jianzhong Wen,[‡,§] Jiro Harada,[∥,@] Kenny Buyle,[§] Kevin Yuan,[‡,§] Hitoshi Tamiaki,[∥] Hirozo Oh-oka,[⊥] Richard A. Loomis,[§] and Robert E. Blankenship*[,‡,§]

[‡]*Department of Biology, and* [§]*Department of Chemistry, Washington University, St. Louis, Missouri 63130,* [∥]*Department of Bioscience and Biotechnology, Faculty of Science and Engineering, Ritsumeikan University, Kusatsu, Shiga 525-8577, Japan, and* [⊥]*Department of Biological Sciences, Graduate School of Science, Osaka University, Osaka 560-0043, Japan.* [@]*Present address: Department of Medical Biochemistry, Kurume University School of Medicine, Fukuoka 830-0011, Japan.*

Received May 2, 2010; Revised Manuscript Received June 1, 2010

ABSTRACT: The Fenna−Matthews−Olson light-harvesting antenna (FMO) protein has been a model system for understanding pigment−protein interactions in the energy transfer process in photosynthesis. All previous studies have utilized wild-type FMO proteins from several species. Here we report the purification and characterization of the first FMO protein variant generated via replacement of the esterifying alcohol at the C-17 propionate residue of bacteriochlorophyll (BChl) *a*, phytol, with geranylgeraniol, which possesses three more double bonds. The FMO protein still assembles with the modified pigment, but both the whole cell absorption and the biochemical purification indicate that the mutant cells contain a much less mature FMO protein. The gene expression was checked using qRT-PCR, and none of the genes encoding BChl *a*-binding proteins are strongly regulated at the transcriptional level. The smaller amount of the FMO protein in the mutant cell is probably due to the degradation of the apo-FMO protein at different stages after it does not bind the normal pigment. The absorption, fluorescence, and CD spectra of the purified FMO variant protein are similar to those of the wild-type FMO protein except the conformations of most pigments are more heterogeneous, which broadens the spectral bands. Interestingly, the lowest-energy pigment binding site seems to be unchanged and is the only peak that can be well resolved in 77 K absorption spectra. The excited-state lifetime of the variant FMO protein is unchanged from that of the wild type and shows a temperature-dependent modulation similar to that of the wild type. The variant FMO protein is less thermally stable than the wild type. The assembly of the FMO protein and also the implications of the decreased FMO/chlorosome stoichiometry are discussed in terms of the topology of these two antennas on the cytoplasmic membrane.

In the photosynthetic green sulfur bacteria, light absorbed by the large peripheral antenna complex called the chlorosome (*1*−*4*) is transferred through the baseplate protein CsmA (*5*−*7*) and the FMO[1] protein (*8*) to the reaction center (RC) where charge separation occurs (*9*). The FMO protein forms a bridge to connect the chlorosome to the cytoplasmic membrane structurally and functionally to direct the excitation energy collected from the chlorosome to the RC (*10*, *11*). Ever since the FMO protein was first discovered in the early 1960s (*12*) and its atomic-resolution structure was determined in the 1970s (*13*), the analysis of this protein has been a major source of our understanding of how pigments bind to photosynthetic proteins and the nature of pigment−pigment interactions.

The FMO protein is a water-soluble protein that is remarkably stable. This makes it a very attractive system for structural and functional studies. The X-ray structures of the FMO protein have been determined from two species of green sulfur bacteria, *Prosthecochloris aestuarii* and *Chlorobaculum tepidum* (*14*−*18*), and a third FMO protein structure from *Pelodictyon phaeum* in which bacteriochlorophyll *e* is the dominant chlorosomal pigment has recently been completed in collaboration with J. Allen and co-workers (unpublished data). The FMO protein forms a compact trimer with 3-fold symmetry (Figure 1A). A large portion of the protein scaffold is β-sheet secondary structure, which forms a "taco shell" to create a highly hydrophobic cavity to hold seven BChl *a* molecules in each monomer. Three monomers join together by both electrostatic and hydrophobic interactions to form a stable structure (*16*). The seven BChl *a* molecules hold very specific conformations inside the protein with their bacteriochlorin rings forming hydrogen bonds and axial ligation with the surrounding protein and water. The tails of

†This work was supported by U.S. Department of Energy Grant DE-FG02-07ER15846 to R.E.B., a Grant-in-Aid for Scientific Research (A) (22245030) from the Japan Society for the Promotion of Science to H.T., a Grant-in-Aid for Scientific Research (C) (21570168) from the Ministry of Education, Culture, Sports, Science, and Technology (MEXT) of Japan to H.O., and a David and Lucile Packard Foundation Fellowship in Science and Engineering to R.A.L. This research is from the Photosynthetic Antenna Research Center (PARC), an Energy Frontier Research Center funded by the U.S. Department of Energy, Office of Science, Office of Basic Energy Sciences, via Grant DE-SC 0001035.

*To whom correspondence should be addressed: Departments of Biology and Chemistry, Campus Box 1137, Washington University, St. Louis, MO 63130. Phone: (314) 935-7971. Fax: (314) 935-4432. E-mail: blankenship@wustl.edu.

[1]Abbreviations: FMO, Fenna−Matthews−Olson bacteriochlorophyll *a*; BChl *a*, bacteriochlorophyll *a*; CD, circular dichroism; RC, reaction center; BChl a_P, BChl *a* with a phytol tail; BChl a_{GG}, BChl *a* with a geranylgeraniol tail; OD, optical density; TCSPC, time-correlated single-photon counting; fwhm, full width at half-maximum; qRT-PCR, quantitative real-time PCR; RT, room temperature; IRF, instrument response function; PDB, Protein Data Bank.

© 2010 American Chemical Society
Published on Web 06/03/2010

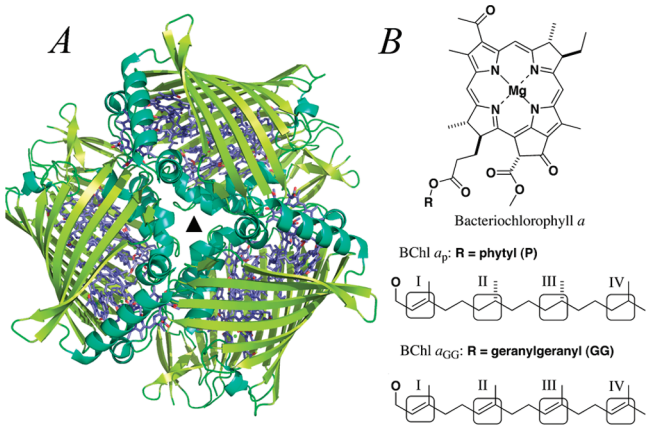

FIGURE 1: (A) Structure of the FMO protein from *C. tepidum* (PDB entry 3ENI). (B) Bacteriochlorophyll *a* (BChl *a*) with phytyl (P) and geranylgeranyl (GG) tails.

the BChl *a* also have unique orientations and may play important structural roles, which have never been elucidated. Recently, the structure of FMO from *P. aestuarii* was determied at 1.3 Å resolution, under which almost every individual non-hydrogen atom could be resolved (*15*). Surprisingly, an eighth BChl *a* was discovered in the monomer connection region, although it had long been known to crystallographers who determined the structures that there was unresolved electron density between the subunits (*14*) and a preliminary report from Nelson and co-workers had suggested that another pigment was in this position (*17*). A comparison of the binding region in the refined FMO structures from *C. tepidum* and *P. aestuarii* allowed Tronrud et al. (*15*) to recognize a specific binding motif and possible structural change for binding the eighth pigment in the two species. Site-directed mutations of the FMO protein will improve our understanding of these issues, although such mutants have not yet been produced.

The FMO protein is quite highly conserved, with levels of amino acid sequence identity among the various green sulfur bacteria typically on the order of 80%. It has been used as a marker gene to classify green sulfur bacteria (*19*, *20*). The known structures are also very similar, but the optical properties, such as 77 K absorption, linear, and circular dichroism, show some differences, the reasons for which are not well understood.

Recently, a sixth phylum of phototrophic bacteria has been discovered in hot springs from Yellowstone National Park (*21*). Remarkably, this organism, *Candidatus Chloracidobacterium thermophilum*, which is a member of the acidobacteria, also contains a clear homologue of the FMO protein. However, this FMO protein is significantly diverged from the ones found in the green sulfur bacteria and is only ~50% identical with the green sulfur FMO proteins (*22*). This FMO protein also has somewhat different spectral features (*22*), which provides an attractive system for comparative studies.

Because of the relatively small number of pigments coupled in the protein and especially the ability to partially resolve the exciton peaks at low temperatures, the FMO protein has been an interesting system for both theoretical and spectroscopic studies in understanding the dynamics of the energy transfer process (*23*−*26*). The prediction of the site energies of individual pigments has been developed from the initial simple fitting of the experimental spectra (*27*, *28*) to direct quantum calculations based on the detailed structures (*11*, *29*). General optical features, such as steady-state spectra and dynamic energy transfer, have been explained, and functions of specific amino acids have been predicted (*29*), although these have not been experimentally verified. All these achievements have on one hand deepened our understanding of light harvesting process, while on the other hand, they have raised interesting questions and provided targets for future mutagenesis studies.

Recently, the FMO protein was used as a model system in the development of the two-dimensional (2D) electronic spectroscopy pioneered in the Fleming group (*30*−*32*). The pathway of energy flow within the molecule was determined by observing off-diagonal peaks in the 2D spectrum, which directly reveal the strength of the excitonic coupling of the pigments (*30*). Later, a long-lived quantum coherence effect in the FMO protein was observed (*33*−*35*) and also in another light-harvesting antenna called PC645 (*36*). These findings have generated intense interest in many areas of science, including discussions of possible relevance to quantum computing (*37*−*40*). Interesting questions include how nature manipulates the specific pigment−protein architecture to preserve such long-lived coherence, and how we can control it. The ability to produce specific FMO protein mutants should provide insights into these issues.

The genome of *C. tepidum* has been sequenced (*41*) and analyzed in detail (*42*). The genetic system in *C. tepidum*, first developed by Wahland and Madigan (*43*), has been developed significantly by Bryant and co-workers (*2*, *42*, *44*). However, the desirable FMO mutants have never been able to be generated, probably because *fmoA* is an essential gene for photosynthesis and the green sulfur bacteria are obligate photoautotrophs. The previous *fmoA* knockout attempts led to cell death. Here we report the first FMO complex mutant, which was generated by replacement of the phytyl at the C-17 propionate residue of the BChl *a* (BChl a_P) with geranylgeranyl (BChl a_{GG}) (Figure 1B) via deletion of the geranylgeranyl reductase (*bchP*) gene (*45*, *46*). Properties of this FMO protein variant are the subject of this paper.

EXPERIMENTAL PROCEDURES

C. tepidum Mutagenesis, Culture Conditions, and FMO Purification. The *C. tepidum bchP* deletion mutant conferring resistance to gentamycin was generated using the method of Harada et al. (*45*). Both the wild-type and mutant cells were grown in sealed carboys at a light intensity of 150 μE m^{-2} s^{-1} at 35 °C for 2 days. For the *bchP* mutant, 5 μM gentamycin was added to the growth medium. Thirty grams of wet cells of *C. tepidum* wild type and *bchP* mutant were used for the FMO purification following the method described by Wen et al. (*10*). The cells were broken by ultrasonication, and the cytoplasmic membranes were enriched by ultracentrifugation. Both membranes were suspended into 150 mL of 20 mM Tris-HCl buffer (pH 8.0), which gave an OD_{745} of ~150 cm^{-1}. The FMO protein was released from the resuspended membrane by incubation with 0.2 M Na_2CO_3 for 24 h and 0.4 M Na_2CO_3 for an additional 24 h. The released FMO protein was collected in the supernatant after ultracentrifugation. The OD_{808} values of the supernatant from the wild-type and mutant cells were 1.6 and 0.3 cm^{-1}, respectively. The protein was further purified by a combination of ion exchange and gel filtration columns until $OD_{267}/OD_{371} < 0.6$.

Pigment Analysis by HPLC. The pigment from the purified FMO protein was extracted by methanol and applied to an Agilent series 1100C high-performance liquid chromatography (HPLC) system with an XDB C18 reversed-phase column

(4.6 mm × 250 mm; pore size, 100 Å; Agilent Technologies). Pigments were eluted by 100% methanol with a flow rate of 1 mL/min for 25 min. The photodiode array detector was set to detect 770, 670, 490, and 280 nm. Pigments eluted by HPLC were collected for further mass analysis.

Pigment Analysis by MALDI-TOF. The pigment fractions collected after HPLC were dried with a speed vac (Millipore) and resuspended into methanol to an OD_{777} of 5. One microliter of pigment solution was mixed with 1 μL of matrix (10 mg/mL 2′,4′,6′-trihydroxyacetophenone monohydrate in 50% CH_3CN/H_2O and 0.1% trifluoroacetic acid) by vortexing, and 0.3 μL was spotted on an ABI-192-AB stainless steel plate. The samples were analyzed using a MALDI-TOF (Applied Biosystems 4700 proteomics analyzer) instrument under reflection positive acquisition and processing modes. Each spectrum was averaged by summing 40 subspectra with 50 laser shots per subspectrum. The laser intensity was 3800 arbitrary units (AU). For the MS/MS experiment, a precursor ion was selected with a molecular weight ± 2 window, and reflection positive MS/MS acquisition and processing modes were used. The laser intensity was increased to 6700 AU. Collision-induced dissociation was applied to fragment the precursor ions. The expansion chamber pressure was maintained at 570 Torr during the MS/MS experiment.

Steady-State Optical Spectra. Absorption spectra were recorded with a Lambda 950 UV/vis spectrophotometer (Perkin-Elmer). Fluorescence emission spectra were recorded using a Photon Technology International fluorometer at a 4 nm spectral bandwidth with an avalanche photodiode detector (model 27, Advanced Photonics Inc.). The excitation wavelength was 370 nm with a 350−540 nm pass-through filter. A 1 cm path length cuvette was used, and the absorption of the samples at 807 nm was 0.1. CD spectra were recorded on a Jasco J-815 CD spectrometer using a 0.1 cm path length quartz cell and were averaged over eight scans for each sample with a scan speed of 50 nm/min and a bandwidth of 1 nm. The protein solution was diluted into 70% glycerol and cooled to 77 K using a temperature-controlled cryostat (OptistatDN, Oxford Instruments) for low-temperature measurements.

Fluorescence Lifetimes. The excited-state lifetime of the FMO protein was measured by time-correlated single-photon counting (TCSPC). A mode-locked Ti:sapphire laser (Tsunami, Spectra-Physics) pumped by a frequency-doubled Nd:YVO4 laser (Millenia Xs, Spectra Physics) was used to generate light pulses at 740 nm. The Ti:sapphire laser was operated at a repetition rate of 81 MHz with a pulse width of < 120 fs [full width at half-maximum (fwhm)]. The repetition rate was controlled using a pulse picker (3980, Spectra Physics). A frequency doubler was used to generate excitation pulses at an excitation wavelength of 370 nm with pulse durations of < 250 fs. The applied excitation power for all the measurements was 2.2 μW at 800 kHz, corresponding to excitation densities of 1×10^8 to 1×10^9 photons pulse^{-1} cm^{-2} which was chosen after a range of intensities was tested to make certain no excitation annihilation effects were present (SI-Figure 3 of the Supporting Information). This was checked by making certain that the fluorescence intensity scales linearly with the excitation energy in the region and no extra fast lifetime decay component exists. The fluorescence signal was collected in a 90° geometry after passing through a monochromator, and arrival times were stored in 4096 channels of a multichannel photomultiplier analyzer. The excitation light had a bandwidth of 12 nm, and the detection monochromator was set for a bandwidth of 6 nm. The instrument response function of the entire TCSPC system (IRF, 35 ps fwhm) was recorded by measuring the scattered light from a piece of metal placed in the sample chamber. Fluorescence decay curves were fitted to a sum of exponentials, convoluted with the instrument response function. The quality of a fit was judged from the χ^2 value and by visual inspection of the residuals. The number of exponentials was considered sufficient if the addition of one extra decay component did not significantly improve the fit.

Table 1: ΔC_T and $\Delta\Delta C_T$ Values of Selected Genes in qRT-PCR

gene	ΔC_T (wild type)	ΔC_T (*bchP*)	$\Delta\Delta C_T$
16S rRNA	0	0	0
csmA	6.4 ± 0.3	6.4 ± 0.3	0 ± 0.3
csmD	8.0 ± 0.2	7.9 ± 0.4	−0.1 ± 0.4
pscA	8.6 ± 0.5	7.3 ± 0.3	−1.3 ± 0.5
fmo	7.2 ± 0.2	6.3 ± 0.3	−0.9 ± 0.3

Thermal Stability. The thermal stability of the wild-type FMO protein and the variant was investigated by monitoring the decrease in the magnitude of the Q_y peak after the temperature had been increased. Temperature was controlled using the Peltier 1+1 temperature controlling accessory (PerkinElmer), which controls and monitors two electronically thermostated cells placed in the sample compartment of the spectrophotometer. The temperature was increased from 5 to 90 °C in increments of 5 °C. The sample was equilibrated at the desired temperature for 5 min before measurement. The temperature stability was ±0.2 °C. The protein was dissolved in 20 mM Tris buffer with 0.1 M NaCl and was gently stirred.

RNA Purification and qRT-PCR. *C. tepidum* wild-type and mutant cells were harvested after growing for 2 days under the same conditions. RNA purification and qRT-PCR were conducted following the methods of Tang et al. (*47*). In brief, RNA was isolated from the cell pellets using TRIzol reagent (Invitrogen) and possible DNA contamination was further removed by DNase treatment. Three independent RNA samples were prepared with an OD_{260}/OD_{280} ratio of > 2. cDNA was synthesized from 1 μg of RNA and 100 μM random 9-mer DNA using Superscript III reverse transcriptase (Invitrogen). The qRT-PCRs were performed via the ABI 7500 real-time PCR system. The primers for qRT-PCRs (shown in SI-Table 1 of the Supporting Information) were designed using Primer Express version 2.0 (Applied Biosystems) and analyzed with Oligo-Analyzer version 3.0 (Integrated DNA Technologies). An initial denaturation step (15 min at 95 °C), followed by 40 amplification cycles (15 s at 95 °C, 30 s at 60 °C, and 45 s at 72 °C), and then one dissociation cycle (15 s at 95 °C, 1 min at 60 °C, and 15 s at 95 °C) were applied for the PCR using Power SYBR green master mix (Applied Biosystems). In the data analysis, the threshold cycle (C_T) was calculated as the cycle number at which ΔRn (the magnitude of the fluorescence intensity generated by the given set of PCRs) crossed the baseline. Data were normalized by calculating $\Delta C_T = C_T$ of the target gene $- C_T$ of the housekeeping gene (16S rRNA). Each experiment was repeated three times for validation, and the mean value was reported (Table 1).

RESULTS

Cell Absorption and Biochemical Purification Indicate Less FMO Protein Is Present in the Mutant Cells. Conversion of the phytyl tail of the BChl *a* (also the primary electron acceptor chlorophyll *a* in the RC) to geranylgeranyl did not

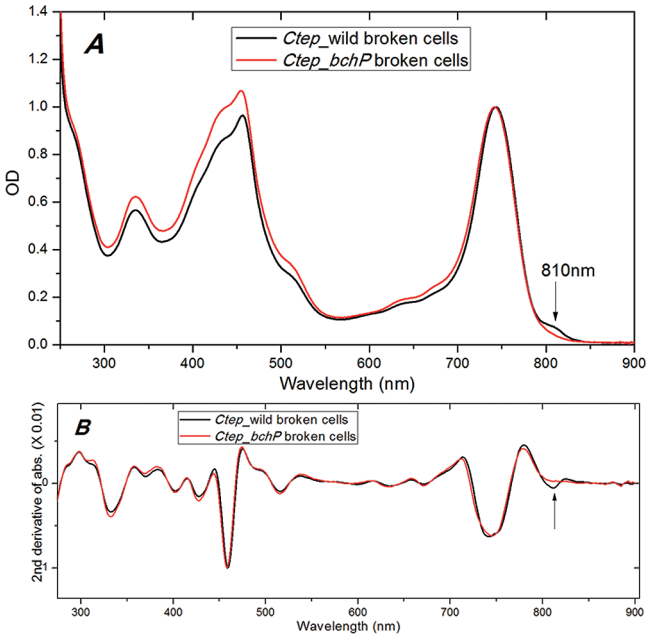

FIGURE 2: (A) Absorption of broken whole cells. Wild-type cells show a shoulder in the 810 nm region that is the Q_y peak of the FMO protein. There is almost no shoulder in the *bchP* cells. (B) Second derivative of the broken whole cell absorption showing the absence of the 810 nm shoulder in the *bchP* cells.

induce a lethal defect in the cell growth. The mutant cells grew well and could reach a cell density similar to that of the wild type as reported by Harada et al. (*45*). Figure 2A shows the absorption of the broken whole cells of the wild type and *bchP* mutant after normalization at the chlorosome Q_y peak at 743 nm (also refer to SI-Figure 1 of the Supporting Information for the whole cell absorption). Compared to the wild-type cells, the *bchP* cells have a higher carotenoid peak in the 400−500 nm region which overlaps with the Soret band of chlorosomes. The FMO shoulder at ~810 nm is almost invisible in the mutant cells. The difference was also clearly shown in the corresponding second derivative of the absorption of the broken whole cells. It is clear that if there is any intact FMO complex in the *bchP* cells, the amount is small compared to the amount of wild type, although there is another possibility that the FMO protein in the *bchP* mutant cells has a Q_y absorbance spectrum very different from that of the wild type, such as blue-shifted and hidden by the dominant chlorosome peak. This is shown below not to be the case.

An Na_2CO_3 treatment of the *bchP* mutant membrane, performed using the same procedure that was used for purifying the wild-type FMO protein, indicates that there are FMO proteins in the *bchP* cells (as characterized below). The same amounts of *C. tepidum* wild-type and mutant membranes (normalized on the chlorosome peaks) were treated with Na_2CO_3. The supernatants collected after ultracentrifugation from the mutant membrane solution showed FMO-like absorption with an OD_{806} of 0.3, while the supernatant of the wild-type cells has an OD_{806} of 1.6. Approximately one-fifth of the FMO protein could be extracted from the *bchP* mutant membranes compared to the wild-type membranes. The FMO protein (FMO_BChla_{GG}) in the supernatant from the mutant membrane solution was purified until it showed one band on SDS−PAGE and was characterized as shown below.

Pigment Analysis of FMO_BChla_{GG}. Although the previous whole cell pigment analysis by HPLC indicates little or no

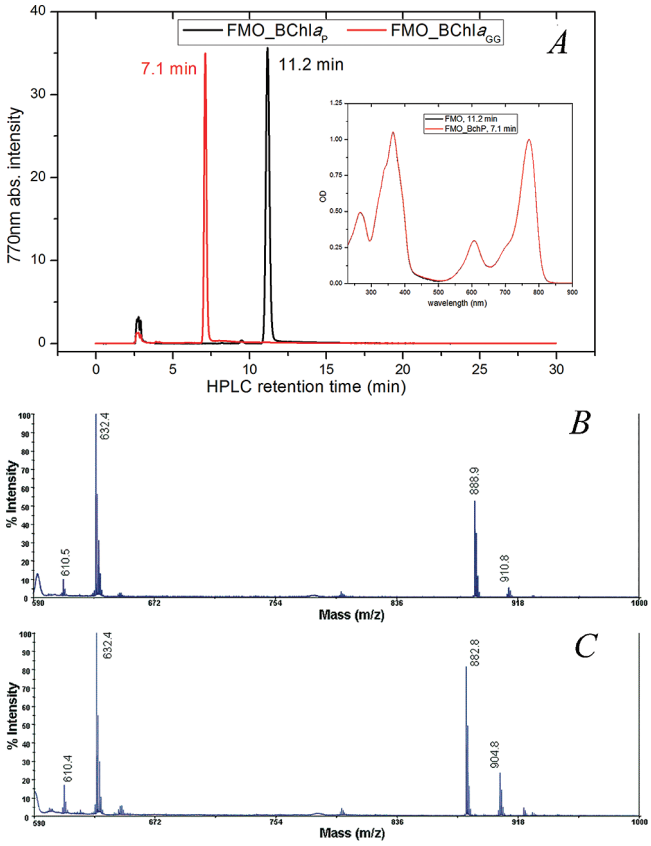

FIGURE 3: (A) HPLC analysis shows the different elution times of pigments in FMO_BChla_P and FMO_BChla_{GG}. Both pigments have a typical BChl *a* absorption as shown in the inset. (B and C) MALDI-TOF mass spectral analysis of the pigments from FMO_BChla_P and FMO_BChla_{GG}, respectively.

BChl a_p in the *bchP* mutant cells (*45*, *46*), we feel it is necessary to check whether the FMO complexes purified from the mutant cells quantitatively incorporated BChl a_{GG} or BChl a_P as the binding pigments. The HPLC analysis of pigments from the purified FMO_BChla_{GG} protein and also the wild-type FMO_BChla_P protein is shown in Figure 3. Under the elution conditions described in Experimental Procedures, the pigment from wild-type FMO_BChla_P elutes at 11 min while that from the *bchP* mutant elutes at 7 min, showing the same absorption as BChl a_P (inset of Figure 3A). Although other detection wavelengths were also monitored, no other elution peaks were observed. Earlier HPLC studies (*45*, *46*, *48*, *49*) have indicated that BChl a_{GG} is less hydrophobic than BChl a_P because of the larger number of double bonds in the tail. Clearly, FMO_BChla_{GG} contains a type of BChl *a* different from BChl a_P, and we anticipate that the peak that elutes at 7 min is BChl a_{GG}. Further identification of the pigment was achieved by mass spectrometry using MALDI-TOF.

To acquire a good mass spectrum of the pigments using MALDI-TOF, we found that 2′,4′,6′-trihydroxyacetophenone monohydrate was a good matrix. The BChl a_P collected from the FMO_BChla_P protein shows four main peaks in the mass spectrum: 910.8, 888.9, 632.4, and 610.5 (Figure 3B). The 910.8 peak corresponds to the monoisotopic peak of BChl a_P ($[C_{55}H_{74}MgN_4O_6]^+$), while the 888.9 peak is BChl a_P with its central Mg replaced by two hydrogen atoms (bacteriopheophytin *a*, BPhe a_P, $[C_{55}H_{76}N_4O_6]^+$). The MS/MS analysis of the 911.8 and 888.9 precursor ions indicate that the loss of the phytyl tails from BChl a_P and BPhe a_P gives rise to the 632.4 (bacteriochlorophyllide *a*, $[C_{35}H_{36}MgN_4O_6]^+$) and 610.5 (bacteriopheophorbide *a*, $[C_{35}H_{38}N_4O_6]^+$) peaks, respectively, as

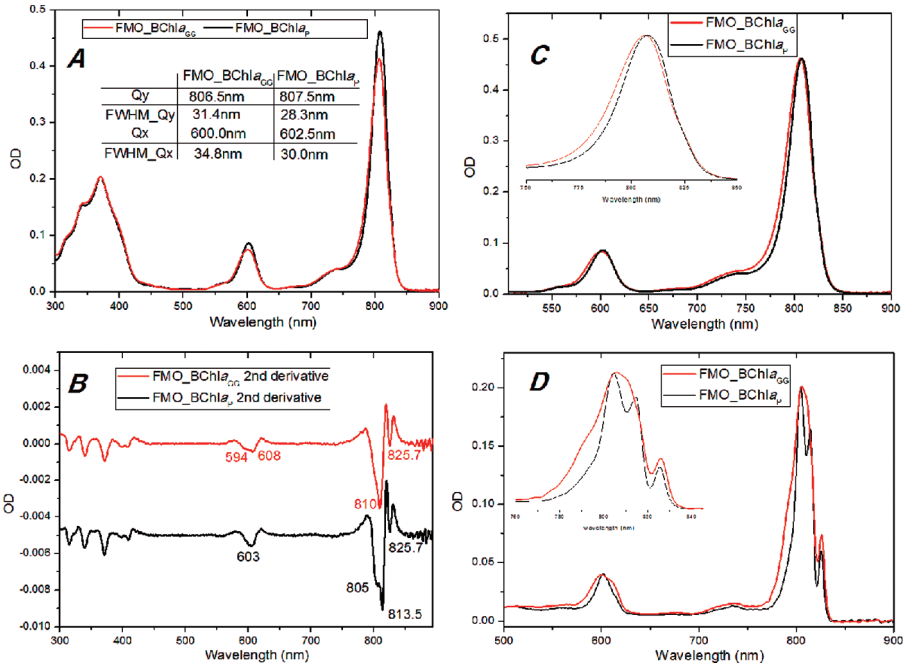

FIGURE 4: (A) RT absorption spectra of FMO_BChla_{GG} and FMO_BChla_P normalized at the Soret bands. Peak positions and bandwidths are shown in the inset. (B) Second derivatives of the absorption spectra of FMO_BChla_{GG} and FMO_BChla_P. (C) Q_y and Q_x regions of the absorptions of FMO_BChla_{GG} and FMO_BChla_P normalized at the Q_y peak (inset). The Q_y and Q_x peaks in the FMO_BChla_{GG} spectrum are blue-shifted and broadened in comparison to those in the FMO_BChla_P spectrum. (D) Absorption spectra (77 K) of FMO_BChla_{GG} and FMO_BChla_P. The Q_y region is expanded in the inset.

shown in SI-Figure 2 of the Supporting Information by MS/MS analysis of the 911.8 and 888.9 precursor ions. The pigment collected from FMO_BChla_{GG} shows a similar mass pattern with four main peaks at 904.8, 882.8, 632.4, and 610.4 (Figure 3C). The 904.8 and 882.8 peaks are 6 units below the weights of BChl a_P and BPhe a_P, respectively, and they match the predicted weight of BChl a_{GG} and BPhe a_{GG} very well (*49*). The 6 unit shift arises from the change of the tail since the 632.4 and 610.4 peaks of the macrocycle were also found in BChl a_P (Figure 3B,C and SI-Figure 2 of the Supporting Information). It is consistent that three more double bonds are in the tail of the pigment from FMO_BChla_{GG}. Thus, we conclude that the FMO protein purified from the *bchP* cells assembled with BChl a_{GG}.

Steady-State Spectra of FMO_BChla$_{GG}$. The RT absorption spectra of FMO_BChla_{GG} and FMO_BChla_P are included in Figure 4. The spectra are normalized at the Soret band to facilitate a comparison of the Q_x and Q_y features (Figure 4A). The intensity of the Q_x and Q_y peaks of FMO_BChla_{GG} are weaker than those of the wild type. In addition, FMO_BChla_P shows more structure in the Q_y region, as indicated in the second derivative of absorption (Figure 4B). Three peaks were resolved at 825.7, 813.5, and 805 nm. FMO_BChla_{GG} can clearly resolve the lowest-energy peak at 825.7 nm and a peak at 810 nm with a shoulder on the high-energy side. Interestingly, the Q_x peak of FMO_BChla_{GG} shows more spectral features than that of the wild type, and two clear peaks at 594 and 608 nm were resolved. FMO_BChla_P shows only a single peak at 603 nm.

If the absorption spectra are normalized at the Q_y peak (Figure 4C), it is clear that the bandwidths of the Q_y and Q_x peaks of FMO_BChla_{GG} are larger than those of FMO_BChla_P. The measured values of the full width at half-maximum (fwhm) of Q_y and Q_x peaks of FMO_BChla_P are 28.3 and 30.0 nm, respectively, while they are 31.4 and 34.8 nm for FMO_BChla_{GG}, respectively. The broader spectrum of FMO_BChla_{GG} may indicate more heterogeneous pigment conformations in FMO_BChla_{GG}, which inhomogeneously broaden the peaks. Moreover, the Q_y and Q_x peaks of FMO_BChla_{GG} are also blue-shifted by 1−2 nm compared to the FMO_BChla_P peaks. A similar spectral shift effect was also reported in the *bchP* mutant of RC (*50*), LH1 (*48*), and LH2 (*51*) complexes in purple bacteria.

At 77 K (Figure 4D), the absorption spectrum of the FMO_BChla_P protein contains three distinct peaks at 825, 814, and 804 nm. In contrast, the FMO_BChla_{GG} spectrum has a broad peak at 806 nm with shoulders on both the high- and low-energy sides. Only the lowest-energy peak at 826 nm could be well-resolved, which suggests that the conformation of the corresponding pigment(s) is not affected much by a change in the tail. However, the peak of the lowest-energy band of FMO_BChla_{GG} is shifted ~1 nm to the red (Figure 4D, inset), indicating a slightly lower energy level compared to that of FMO_BChla_P. It is also noted that the Q_x peak of FMO_BChla_{GG} is also much broader than that of the wild type. The 77 K absorption spectrum further confirms a more heterogeneous conformational distribution of all the other pigments, which gave inhomogeneous peak broadening and thus could not be resolved at 77 K.

At RT, the fluorescence spectrum of FMO_BChla_P has an emission peak at 825 nm with a fwhm of 32 nm. The emission peak of FMO_BChla_{GG} is shifted slightly to a higher energy, 822 nm, and is sightly more broad, fwhm of 34 nm (Figure 5A). The broader emission peak of FMO_BChla_{GG} implies that there are more heterogeneous pigment conformations in the variant protein.

In contrast, the emission peak widths of FMO_BChla_{GG} and FMO_BChla_P at 77 K are quite similar with fwhm values of 13.6 and 13.2 nm, respectively (Figure 5B), which is consistent with the conclusion from 77 K absorption that the conformation of the lowest-energy pigment(s) is more similar. However, the emission peak of FMO_BChla_{GG} is slightly red-shifted (1.6 nm)

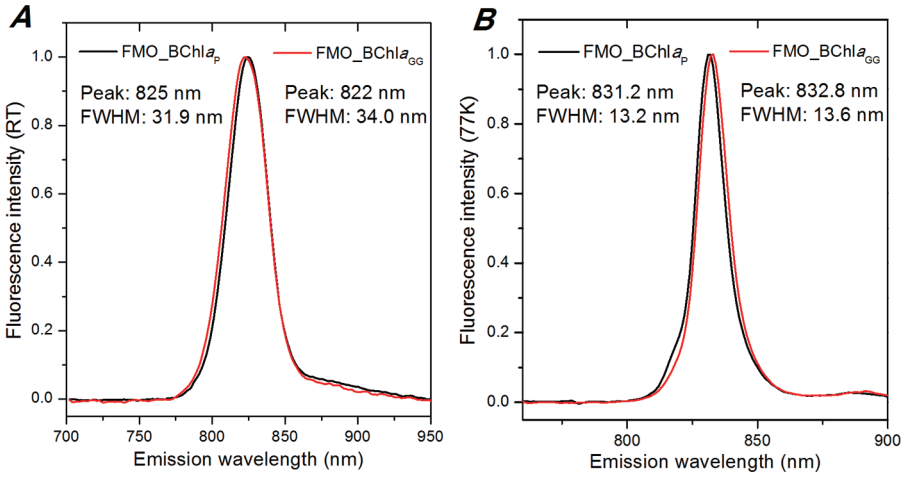

FIGURE 5: Normalized RT (A) and 77 K (B) fluorescence spectra of FMO_BChla_{GG} and FMO_BChla_P (excitation at 370 nm).

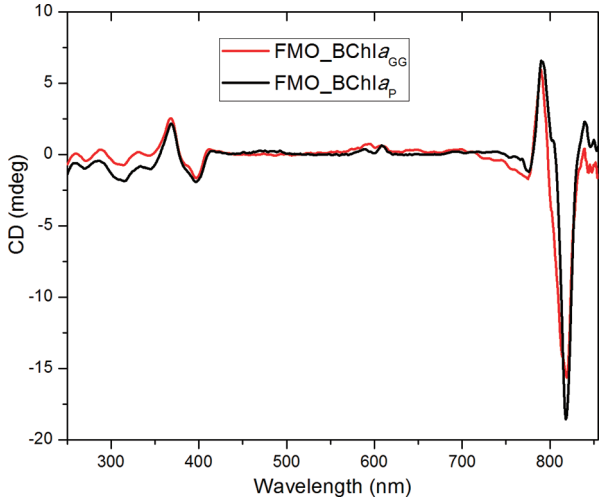

FIGURE 6: CD spectral comparison, normalized at the Soret band absorption.

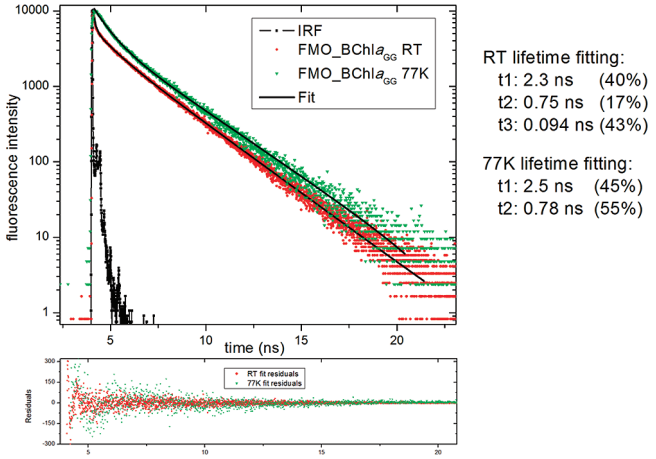

FIGURE 7: RT and 77 K fluorescence decay profiles of FMO_BChla_{GG}. Three exponential decays fit the RT fluorescence kinetics very well. The dominant lifetime components are 94 ps and 2.3 ns, which account for 43 and 40% of the amplitude, respectively. Two exponential decays give a reasonable fit of the 77 K fluorescence decay. The lifetimes increase to 2.5 and 0.78 ns, which account for 45 and 55% of the amplitude, respectively. The bottom panel shows the residuals between the fitting and the experimental data.

compared to that of FMO_BChla_P, which indicates a slightly lower energy level of FMO_BChla_{GG} that was previously suggested in the 77 K absorption spectrum. The larger shift of the FMO_BChla_{GG} fluorescence peak (10.2 nm = 832.8 nm − 822 nm) observed when the temperature is decreased from RT to 77 K in comparison to that of the FMO_BChla_P peak (6.2 nm = 831.2 nm − 825 nm) suggests the energy gap between the two lowest excitonic states is smaller in FMO_BChla_{GG}. Therefore, the population of the second excitonic state is larger in FMO_BChla_{GG} than in wild-type FMO_BChla_P at RT, explaining the larger blue shift of the emission of FMO_BChla_{GG}. At 77 K, the thermal energy is not enough to populate the second excitonic state, and hence, there is emission only from the low-energy state.

The CD spectrum of FMO_BChla_{GG} is similar to that of FMO_BChla_P, except there is a slightly weaker CD signal in the Q_y region (Figure 6). This small difference suggests a weaker excitonic coupling strength for FMO_BChla_{GG} in comparison with that for FMO_BChla_P.

Overall, FMO_BChla_{GG} has steady-state optical properties quite similar to those of FMO_BChla_P except more heterogeneous pigment conformations, which may affect the energy transfer as suggested from the RT and 77 K fluorescence. Interestingly, the lowest excitonic state seems not to be changed significantly. The absence of the 810 nm shoulder in the whole cell absorption spectrum clearly indicates that there is a smaller number of FMO complexes in the mutant, which is consistent with the biochemical purification that *bchP* cells have much less FMO that can be extracted.

Fluorescence Dynamics. The fluorescence decay kinetics of FMO_BChla_{GG} was probed by excitation in the Soret band using TCSPC. In Figure 7, the measured fluorescence decay curves at RT and 77 K and the fitted decay curves, together with the corresponding IRF, are shown. It is clear that the fluorescence decay of FMO_BChla_{GG} at RT (824 nm) is significantly faster than the decay at 77 K. The former can be fitted very well with three exponentials having lifetimes of 2.3 ns (40%), 0.75 ns (17%), and 0.094 ns (43%). The 77 K fluorescence decay (832 nm) can be best described by a biexponential decay with time constants of 2.5 ns (45%) and 0.78 ns (55%). The lifetime of FMO_BChla_P was measured under the same conditions and gave virtually the same results (SI-Figure 4 of the Supporting Information) in agreement with previous reports (*52*). It has long been known that the lifetime of FMO depends on the redox condition of the solution (*53*) and also the temperature (*54*); however, the molecular mechanism of this excited-state modulation is still unclear. Here, a similar

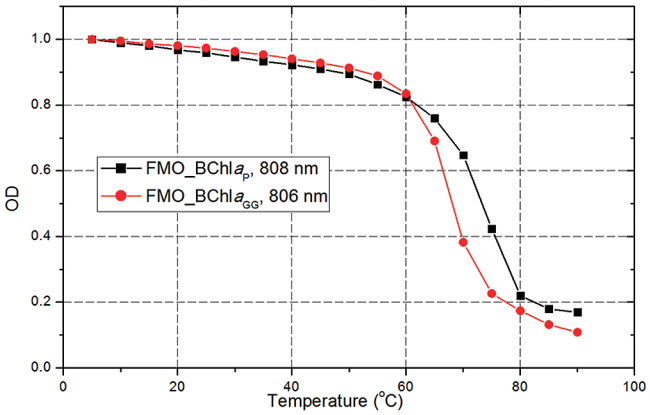

FIGURE 8: Thermal stability of FMO_BChla_{GG} and FMO_BChla_P monitored at the Q_y absorption peaks from 5 to 90 °C with a temperature step size of 5 °C. The solution was equilibrated for 5 min at each temperature point.

temperature-regulated fluorescence lifetime in FMO_BChla_{GG} is observed. The fast decay component, 0.094 ns, of FMO_BChla_{GG} at RT is not observed at 77 K, and the relative contribution of the slow components increased.

Thermal Stability of FMO_BChla$_{GG}$. The *C. tepidum bchP* mutant is observed to grow photosynthetically, although the growth rate decreases with an increase in temperature (*45*). It is possible that the geranylgeranyl tail caused the BChl *a* binding proteins to be unstable at higher temperatures. Therefore, the thermal stability of FMO_BChla_{GG} was studied in comparison with that of FMO_BChla_P by monitoring the amplitude of the Q_y peak in the absorption spectra recorded as a function of temperature. The thermally induced FMO unfolding process was irreversible, so the change in free energy could not be quantified. However, it is still clear that FMO_BChla_{GG} is less thermally stable and has a half-melting point at ~67 °C (Figure 8). FMO_BChla_P, instead, has a half-melting point at ~73 °C (Figure 8). Below 60 °C, the slopes of the melting curves of FMO_BChla_{GG} and FMO_BChla_P are similar. The pigments start to degrade, and the protein forms strong aggregates above 80 °C, which causes the continuous decrease in the absorption in the Q_y region.

Gene Expression Profiles. The expression levels of genes encoding the FMO protein and some other BChl *a* binding or related proteins (CsmA, CsmD, and PscA) were checked by qRT-PCR analysis of the mRNA at the transcriptional level. Normalized ΔC_T data using 16S rRNA as the housekeeping gene from *C. tepidum* wild-type cells were compared to data from *C. tepidum bchP* cells, in which $\Delta\Delta C_T = \Delta C_T^{Ctep\_bchP} - \Delta C_T^{Ctep\_wild}$. If a certain gene is downregulated in the mutant cells, the mRNA level of this gene will be low. In the qRT-PCR, it will need more amplification cycles for this gene to reach the threshold and, thus, give a larger ΔC_T and a positive $\Delta\Delta C_T$ when compared with that of the wild type. As shown in Table 1, the $\Delta\Delta C_T$ values of all the genes are around zero except that of the *pscA* gene which has a slightly negative value. It seems the mRNA levels of all the proteins are not significantly changed except for a small upregulation of the *pscA* gene in the *bchP* mutant. The smaller amount of FMO holoprotein complexes in the *bchP* mutant might be a result of less efficient assembly with the wrong pigment so that the translated FMO apoprotein polypeptide is degraded quickly by the cell. Actually, the ratio of the total FMO polypeptides in the wild-type and *bchP* mutant cells depending on the cell growth phase and the duration of protein processing could range from ~2 to ~6 as seen by the Western blot using an anti-FMO antibody (data not shown).

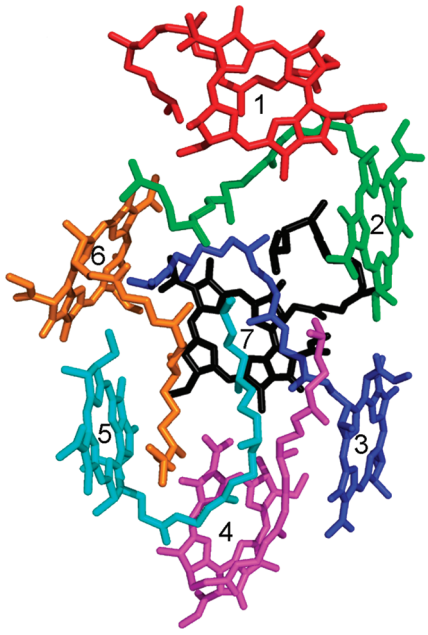

FIGURE 9: Conformation of BChl a_P in an FMO monomer with each pigment highlighted in different colors and numbered. The eighth pigment was omitted because the tail is invisible in the structure.

DISCUSSION

FMO Assembly. The replacement of the phytyl tail in the BChl *a* with geranylgeranyl (Figure 1B) will add more rigidness because of the torsional restrictions from the double bonds. However, the change from phytyl to geranylgeranyl does not introduce a lethal defect with respect to cell growth. In *C. tepidum*, BChl *a* is distributed in the CsmA protein, FMO protein, and the RC. In the crystal structure of the wild-type FMO protein (PDB entries 1M50 and 3ENI), the tails of BChl *a* are tightly packed and have well-defined conformations (Figures 1A and 9). The torsion angles at one double and three single bond positions in BChl a_P from the structures of various wild-type FMO proteins were measured and are listed in SI-Table 2 of the Supporting Information. On the basis of this known information, the conformation of the tail of BChl a_P #4 seems to be less affected if changed from phytyl to geranylgeranyl. The other BChls a_P species seem to have to adopt new conformations to release the torsion restriction if changed from phytyl to geranylgeranyl. Nevertheless, only the torsion angles in regions II and III of certain BChl a_P species will be affected more in the *bchP* mutant since region IV is at the end of the tail which should have more flexibility to adopt the double bond.

Both the whole cell absorption spectra and the biochemical extraction of the FMO protein indicate fewer FMO protein complexes in the *bchP* mutant. However, the expression level of the *fmoA* gene seems to be unchanged on the basis of qRT-PCR measurements. Thus, the smaller amount of native FMO in the mutant probably results from the failure of assembling native FMO complexes because of the unfavorable pigment composition. The lack of atomic-resolution structures for the CsmA and RC makes it difficult to evaluate the BChl *a* binding sites and the assembly of these two proteins. Although at the gene expression level, it seems the *csmA* gene is not regulated and the *pscA* gene is slightly upregulated in the mutant, it will be important in the

future to determine whether there is any regulation at the active protein complex level as was observed in the FMO complex.

There have been several studies that also indicate that the type of esterifying alcohol is an important component for the synthesis of a fully functional photosystem (*48*, *50*, *51*, *55*). For example, it has been observed that the amounts of mature LH2, LH1, and RC complexes in both *Rhodobacter sphaeroides* (*48*) and *Rhodobacter capsulatus* (*50*) were severely reduced after replacement of the phytyl tail of BChl *a* with a geranylgeranyl tail. In an extreme situation, if the tail esterifying step was blocked, no such complexes were assembled and the cells lost the ability to conduct photosynthesis (*50*). The biological significance of the ester groups of the 17-propionate substituent has been recently reviewed by Tamiaki et al. (*55*).

Optical Properties and Thermal Stability. When the favorable BChl a_P is not available, the FMO protein will incorporate the more rigid BChl a_{GG}, albeit less efficiently. This directly results in a partial failure of the protein assembly, as discussed above. Additionally, the conformation of BChl a_{GG} in the assembled FMO variant is more heterogeneously distributed, which broadens the spectral peak inhomogeneously. This broadening was observed in both the absorption and fluorescence spectra recorded at RT and 77 K (Figures 4 and 5). Interestingly, the only excitonic state that can be resolved at 77 K is the 826 nm peak, which is the excitation trap. As discussed above, the conformation of BChl *a* #4, which partially contributed to the lowest excitonic state (*26*, *27*), seems to be unchanged. Lastly, although there are some FMO proteins successfully assembled, they are still slightly less thermally stable than the wild type (Figure 8).

Because the tail is not part of the conjugated electron system of the tetrapyrrole, it is commonly accepted to be neutral and optically silent (*55*, *56*). The difference in the spectra of the wild-type and mutant FMOs is probably due to an altered packing of the BChl to release the torsion restriction, resulting in changes in the interactions between BChl and other components of the FMO protein.

Membrane Topology. The smaller number of mature FMO complexes in the *bchP* mutant cells results in a significant change in the stoichiometry of the chlorosome to FMO, which might give us some indication of the relative distribution of the chlorosome and FMO on the membrane. The purified chlorosomes from both the wild-type and mutant cells are similar in size as checked by sucrose density gradients (data not shown). If all the FMO proteins are covered by the chlorosomes in vivo, the FMO complexes on the cytoplasmic membrane in the *bchP* cells should be more loosely packed than those of the wild type. It will be interesting to compare the binding affinity of the chlorosome to the cytoplasmic membrane and the stoichiometry of CsmA to FMO in the *C. tepidum* wild-type and *bchP* mutant cells. However, if the number of FMO proteins under the chlorosome is the same, the smaller amount of FMO protein in the mutant cells must mean that there are FMO proteins that are not covered by the chlorosome, at least in the wild-type cells. It has been widely discussed in terms of how many FMO proteins per RC are present in the wild-type RC (*57*, *58*), with the numbers ranging from five to six to only one FMO tightly bound to the RC. The *bchP* mutant may be a good comparison system for reinvestigating this question in the future.

In conclusion, the success in generating an FMO variant by replacing the phytyl tail of BChl *a* with geranylgeranyl allows us to examine the assembly of the FMO protein. Although the FMO protein could still be assembled, the amount seems to be much smaller in the mutant cells, which raises interesting questions about the distribution of FMO relative to the chlorosomes on the cell membrane. The assembled FMO variant shows optical properties generally similar to those of the wild type, but the conformations of the pigments are more heterogeneously distributed because of the rigidness of more double bonds, as seen in the spectral broadening. An atomic-resolution structure of FMO_BChla_{GG} will be extremely helpful in understanding the structural and functional differences compared to the wild-type FMO protein.

ACKNOWLEDGMENT

We thank Drs. Yueyong Xin and Aaron M. Collins for discussion. We thank Barbara Honchak for help in running Western blots and Xianglu Li for suggestions for running qRT-PCR. We also thank the Washington University Mass Spectrometry Resource Center for assistance, supported by NIH NCRR Grant 2P41RR000954.

SUPPORTING INFORMATION AVAILABLE

Whole cell absorption of wild-type and mutant cells, details of TCSPC lifetime measurements, and list of torsion angels of the tails of BChl a_P in various FMO structures. This material is available free of charge via the Internet at http://pubs.acs.org.

REFERENCES

1. Ganapathy, S., Oostergetel, G. T., Wawrzyniak, P. K., Reus, M., Gomez Maqueo Chew, A., Buda, F., Boekema, E. J., Bryant, D. A., Holzwarth, A. R., and de Groot, H. J. (2009) Alternating syn-anti bacteriochlorophylls form concentric helical nanotubes in chlorosomes. *Proc. Natl. Acad. Sci. U.S.A. 106*, 8525–8530.
2. Frigaard, N. U., Li, H., Milks, K. J., and Bryant, D. A. (2002) Nine mutants of *Chlorobium tepidum* each unable to synthesize a different chlorosome protein still assemble functional chlorosomes. *J. Bacteriol. 186*, 646–653.
3. Oostergetel, G. T., van Amerongen, H., and Boekema, E. J. (2010) The chlorosome: A prototype for efficient light harvesting in photosynthesis. *Photosynth. Res. 104*, 245–255.
4. Saga, Y., Shibata, Y., and Tamiaki, H. (2010) Spectral properties of single light-harvesting complexes in bacterial photosynthesis. *J. Photochem. Photobiol., C 11*, 15–24.
5. Pedersen, M. O., Linnanto, J., Frigaard, N. U., Nielsen, N. C., and Miller, M. (2010) A model of the protein-pigment baseplate complex in chlorosomes of photosynthetic green bacteria. *Photosynth. Res. 104*, 233–243.
6. Pedersen, M. Ø., Underhaug, J., Dittmer, J., Miller, M., and Nielsen, N. C. (2008) The three-dimensional structure of CsmA: A small antenna protein from the green sulfur bacterium *Chlorobium tepidum*. *FEBS Lett. 582*, 2869–2874.
7. Montaño, G. A., Wu, H. M., Lin, S., Brune, D. C., and Blankenship, R. E. (2003) Isolation and characterization of the B798 light-harvesting baseplate from the chlorosomes of *Chloroflexus aurantiacus*. *Biochemistry 42*, 10246–10251.
8. Olson, J. M. (2004) The FMO protein. *Photosynth Res 80*, 181–187.
9. Hauska, G., Schoedl, T., Remigy, H., and Tsiotis, G. (2001) The reaction center of green sulfur bacteria. *Biochim. Biophys. Acta 1507*, 260–277.
10. Wen, J., Zhang, H., Gross, M. L., and Blankenship, R. E. (2009) Membrane orientation of the FMO antenna protein from *Chlorobaculum tepidum* as determined by mass spectrometry-based footprinting. *Proc. Natl. Acad. Sci. U.S.A. 106*, 6134–6139.
11. Adolphs, J., and Renger, T. (2006) How proteins trigger excitation energy transfer in the FMO complex of green sulfur bacteria. *Biophys. J. 91*, 2778–2797.
12. Olson, J., and Romano, C. (1962) A new chlorophyll from green bacteria. *Biochim. Biophys. Acta 59*, 726–728.
13. Fenna, R. E., and Matthews, B. W. (1975) Chlorophyll arrangement in a bacteriochlorophyll protein from *Chlorobium limicola*. *Nature 258*, 573–577.
14. Tronrud, D. E., Schmid, M. F., and Matthews, B. W. (1986) Structure and X-ray amino acid sequence of a bacteriochlorophyll *a* protein from *Prosthecochloris aestuarii* refined at 1.9 Å resolution. *J. Mol. Biol. 188*, 443–454.
15. Tronrud, D. E., Wen, J., Gay, L., and Blankenship, R. E. (2009) The structural basis for the difference in absorbance spectra for the FMO

antenna protein from various green sulfur bacteria. *Photosynth. Res. 100*, 79–87.
16. Li, Y. F., Zhou, W., Blankenship, R. E., and Allen, J. P. (1997) Crystal structure of the bacteriochlorophyll *a* protein from *Chlorobium tepidum*. *J. Mol. Biol. 271*, 456–471.
17. Ben-Shem, A., Frolow, F., and Nelson, N. (2004) Evolution of photosystem I: From symmetry through pseudo-symmetry to asymmetry. *FEBS Lett. 564*, 274–280.
18. Camara-Artigas, A., Blankenship, R. E., and Allen, J. P. (2003) The structure of the FMO protein from *Chlorobium tepidum* at 2.2 Å resolution. *Photosynth. Res. 75*, 49–55.
19. Alexander, B., Andersen, J. H., Cox, R. P., and Imhoff, J. F. (2002) Phylogeny of green sulfur bacteria on the basis of gene sequences of 16S rRNA and of the Fenna-Matthews-Olson protein. *Arch. Microbiol. 178*, 131–140.
20. Imhoff, J. F. (2003) Phylogenetic taxonomy of the family Chlorobiaceae on the basis of 16S rRNA and *fmo* (Fenna-Matthews-Olson protein) gene sequences. *Int. J. Syst. Evol. Microbiol. 53*, 941–951.
21. Bryant, D. A., Costas, A. M., Maresca, J. A., Chew, A. G., Klatt, C. G., Bateson, M. M., Tallon, L. J., Hostetler, J., Nelson, W. C., Heidelberg, J. F., and Ward, D. M. (2007) *Candidatus Chloracidobacterium thermophilum*: An aerobic phototrophic Acidobacterium. *Science 317*, 523–526.
22. Tsukatani, Y., Wen, J., Blankenship, R. E., and Bryant, D. A. (2010) Characterization of the FMO protein from the aerobic chlorophototroph, *Candidatus* Chloracidobacterium thermophilum. *Photosynth. Res. 104*, 201–209.
23. Cheng, Y. C., and Fleming, G. R. (2009) Dynamics of Light Harvesting in Photosynthesis. *Annu. Rev. Phys. Chem. 60*, 241–262.
24. Milder, M. T. W., Brüggemann, B., van Grondelle, R., and Herek, J. L. (2010) Revisiting the optical properties of the FMO protein. *Photosynth. Res. 104*, 257–274.
25. Renger, T. (2009) Theory of excitation energy transfer: From structure to function. *Photosynth. Res. 102*, 471–485.
26. Blankenship, R. E., and Matsuura, K. (2003) Antenna complexes from green photosynthetic bacteria. In Light-Harvesting Antenna in Photosynthesis (Green, B. R., and Parson, W. W., Eds.) pp 195−217, Kluwer Academic Publishers, Dordrecht, The Netherlands.
27. Johnson, S., and Small, G. (1991) Excited-state structure and energy-transfer dynamics of the bacteriochlorophyll *a* antenna complex from *Prosthecochloris aestuarii*. *J. Phys. Chem. 95*, 471–479.
28. Pearlstein, R. (1992) Theory of the optical spectra of the bacteriochlorophyll *a* antenna protein trimer from *Prosthecochloris aestuarii*. *Photosynth. Res. 31*, 213–226.
29. Müh, F., Madjet, Mel-A, Adolphs, J., Abdurahman, A., Rabenstein, B., Ishikita, H., Knapp, E. W., and Renger, T. (2007) α-Helices direct excitation energy flow in the Fenna-Matthews-Olson protein. *Proc. Natl. Acad. Sci. U.S.A. 104*, 16862–16867.
30. Brixner, T., Stenger, J., Vaswani, H. M., Cho, M., Blankenship, R. E., and Fleming, G. R. (2005) Two-dimensional spectroscopy of electronic couplings in photosynthesis. *Nature 434*, 625–628.
31. Read, E. L., Schlau-Cohen, G. S., Engel, G. S., Wen, J., Blankenship, R. E., and Fleming, G. R. (2008) Visualization of Excitonic Structure in the Fenna-Matthews-Olson Photosynthetic Complex by Polarization-Dependent Two-Dimensional Electronic Spectroscopy. *Biophys. J. 95*, 847–856.
32. Cho, M., Brixner, T., Stiopkin, I., Vaswani, H., and Fleming, G. R. (2006) Two Dimensional Electronic Spectroscopy of Molecular Complexes. *J. Chin. Chem. Soc. 53*, 15–24.
33. Engel, G. S., Calhoun, T. R., Read, E. L., Ahn, T. K., Mančal, T, Cheng, Y. C., Blankenship, R. E., and Fleming, G. R. (2007) Evidence for wavelike energy transfer through quantum coherence in photosynthetic systems. *Nature 446*, 782–786.
34. Ishizaki, A., and Fleming, G. R. (2009) Theoretical examination of quantum coherence in a photosynthetic system at physiological temperature. *Proc. Natl. Acad. Sci. U.S.A. 106*, 17255–17260.
35. Panitchayangkoon, G., Hayes, G., Fransted, K. A., Caram, J. R., Harel, E., Wen, J., Blankenship, R. E., and Engel, G. S. (2010) Long-lived quantum coherence in photosynthetic complexes at physiological temperature. *arXiv:1001.5108v1* .
36. Collini, E., Wong, C. Y., Wilk, K. E., Curmi, P. M. G., Brumer, P., and Scholes, G. D. (2010) Coherently wired light-harvesting in photosynthetic marine algae at ambient temperature. *Nature 463*, 644–648.
37. Mohseni, M., Rebentrost, P., Lloyd, S., and Aspuru-Guzik, A. (2008) Environment-assisted quantum walks in energy transfer of photosynthetic complexes. *J. Chem. Phys. 129*, 174106.
38. Beljonne, D., Curutchet, C., Scholes, G. D., and Silbey, R. J. (2009) Beyond Forster Resonance Energy Transfer in Biological and Nanoscale Systems. *J. Phys. Chem. B 113*, 6583–6599.
39. Palmieri, B., Abramavicius, D., and Mukamel, S. (2010) Interplay of slow bath fluctuations and energy transfer in 2D spectroscopy of the FMO light-harvesting complex: Benchmarking of simulation protocols. *Phys. Chem. Chem. Phys. 12*, 108–114.
40. Rebentrost, P., Mohseni, M., and Aspuru-Guzik, A. (2009) Role of Quantum Coherence and Environmental Fluctuations in Chromophoric Energy Transport. *J. Phys. Chem. B 113*, 9942–9947.
41. Eisen, J. A., Nelson, K. E., Paulsen, I. T., Heidelberg, J. F., Wu, M., Dodson, R. J., Deboy, R., Gwinn, M. L., Nelson, W. C., Haft, D. H., Hickey, E. K., Peterson, J. D., Durkin, A. S., Kolonay, J. L., Yang, F., Holt, I., Umayam, L. A., Mason, T., Brenner, M., Shea, T. P., Parksey, D., Nierman, W. C., Feldblyum, T. V., Hansen, C. L., Craven, M. B., Radune, D., Vamathevan, J., Khouri, H., White, O., Gruber, T. M., Ketchum, K. A., Venter, J. C., Tettelin, H., Bryant, D. A., and Fraser, C. M. (2002) The complete genome sequence of *Chlorobium tepidum* TLS, a photosynthetic, anaerobic, green-sulfur bacterium. *Proc. Natl. Acad. Sci. U.S.A. 99*, 9509–9514.
42. Frigaard, N. U., Chew, A. G. M., Li, H., Maresca, J. A., and Bryant, D. A. (2003) *Chlorobium tepidum*: Insights into the structure, physiology and metabolism of a green sulfur bacterium derived from the complete genome sequence. *Photosynth. Res. 78*, 93–117.
43. Wahlund, T. M., and Madigan, M. T. (1995) Genetic transfer by conjugation in the thermophilic green sulfur bacterium *Chlorobium tepidum*. *J. Bacteriol. 177*, 2583–2588.
44. Frigaard, N. U., and Bryant, D. (2004) Seeing green bacteria in a new light: Genomics-enabled studies of the photosynthetic apparatus in green sulfur bacteria and filamentous anoxygenic phototrophic bacteria. *Arch. Microbiol. 182*, 265–276.
45. Harada, J., Miyago, S., Mizoguchi, T., Azai, C., Inoue, K., and Tamiaki, H. (2008) Accumulation of chlorophyllous pigments esterified with the geranylgeranyl group and photosynthetic competence in the CT2256-deleted mutant of the green sulfur bacterium *Chlorobium tepidum*. *Photochem. Photobiol. Sci. 7*, 1179–1187.
46. Chew, A. G. M., Frigaard, N. U., and Bryant, D. A. (2008) Identification of the *bchP* gene, encoding geranylgeranyl reductase in *Chlorobaculum tepidum*. *J. Bacteriol. 190*, 747–749.
47. Tang, K.-H., Wen, J., Li, X., and Blankenship, R. E. (2009) The role of the AcsF protein in *Chloroflexus aurantiacus*. *J. Bacteriol. 191*, 3580–3587.
48. Addlesee, H. A., and Hunter, C. N. (1999) Physical mapping and functional assignment of the geranylgeranyl-bacteriochlorophyll reductase gene, *bchP*, of *Rhodobacter sphaeroides*. *J. Bacteriol. 181*, 7248–7255.
49. Mizoguchi, T., Harada, J., and Tamiaki, H. (2006) Structural determination of dihydro- and tetrahydrogeranylgeranyl groups at the 17-propionate of bacteriochlorophylls-α. *FEBS Lett. 580*, 6644–6648.
50. Bollivar, D. W., Wang, S., Allen, J. P., and Bauer, C. E. (1994) Molecular genetic analysis of terminal steps in bacteriochlorophyll *a* biosynthesis: Characterization of a *Rhodobacter capsulatus* strain that synthesizes geranylgeraniol-esterified bacteriochlorophyll *a*. *Biochemistry 33*, 12763–12768.
51. Addlesee, H. A., and Hunter, C. N. (2002) *Rhodospirillum rubrum* possesses a variant of the *bchP* gene, encoding geranylgeranyl-bacteriopheophytin reductase. *J. Bacteriol. 184*, 1578–1586.
52. Freiberg, A., Lin, S., Timpmann, K., and Blankenship, R. E. (1997) Exciton dynamics in FMO bacteriochlorophyll protein at low temperatures. *J. Phys. Chem. B 101*, 7211–7220.
53. Zhou, W., LoBrutto, R., Lin, S., and Blankenship, R. E. (1994) Redox effects on the bacteriochlorophyll α-containing Fenna-Matthews-Olson protein from *Chlorobium cepidum*. *Photosynth. Res. 41*, 89–96.
54. Rätsep, M., and Freiberg, A. (2007) Unusual temperature quenching of bacteriochlorophyll a fluorescence in FMO antenna protein trimers. *Chem. Phys. Lett. 434*, 306–311.
55. Tamiaki, H., Shibata, R., and Mizoguchi, T. (2007) The 17-propionate function of (bacterio)chlorophylls: Biological implication of their long esterifying chains in photosynthetic systems. *Photochem. Photobiol. 83*, 152–162.
56. Fiedor, L., Kania, A., Myśliwa-Kurdziel, B., Orzeł, Ł., and Stochel, G. (2008) Understanding chlorophylls: Central magnesium ion and phytyl as structural determinants. *Biochim. Biophys. Acta 1777*, 1491–1500.
57. Francke, C., Permentier, H. P., Franken, E. M., Neerken, S., and Amesz, J. (1997) Isolation and properties of photochemically active reaction center complexes from the green sulfur bacterium *Prosthecochloris aestuarii*. *Biochemistry 36*, 14167–14172.
58. Rémigy, H. W., Stahlberg, H., Fotiadis, D., Müller, S. A., Wolpensinger, B., Engel, A., Hauska, G., and Tsiotis, G. (1999) The reaction center complex from the green sulfur bacterium *Chlorobium tepidum*: A structural analysis by scanning transmission electron microscopy. *J. Mol. Biol. 290*, 851–858.